

# Cervical facet joint kinematics during bilateral facet dislocation

Manohar M. Panjabi · Andrew K. Simpson ·  
Paul C. Ivancic · Adam M. Pearson ·  
Yasuhiro Tominaga · James J. Yue

Received: 17 October 2006/Revised: 1 February 2007/Accepted: 14 May 2007/Published online: 14 June 2007  
© Springer-Verlag 2007

**Abstract** Previous biomechanical models of cervical bilateral facet dislocation (BFD) are limited to quasi-static loading or manual ligament transection. The goal of the present study was to determine the facet joint kinematics during high-speed BFD. Dislocation was simulated using ten cervical functional spinal units with muscle force replication by frontal impact of the lower vertebra, tilted posteriorly by 42.5°. Average peak rotations and anterior sliding (displacement of upper articulating facet surface along the lower), separation and compression (displacement of upper facet away from and towards the lower), and lateral shear were determined at the anterior and posterior edges of the right and left facets and statistically compared ( $P < 0.05$ ). First, peak facet separation occurred, and was significantly greater at the left posterior facet edge, as compared to the anterior edges. Next, peak flexion rotation and anterior facet sliding occurred, followed by peak facet compression. The highest average facet translation peaks were 22.0 mm for anterior sliding, 7.9 mm for separation, 9.9 mm for compression and 3.6 mm for lateral shear. The highest average rotation of 63° occurred in flexion,

significantly greater than all other directions. These events occurred, on average, within 0.29 s following impact. During BFD, the main sagittal motions included facet separation, flexion rotation, anterior sliding, followed by compression, however, non-sagittal motions also existed. These motions indicated that unilateral dislocation may precede bilateral dislocation.

**Keywords** Bilateral facet dislocation · Cervical spine · Facet joint · Injury mechanism · Kinematics

## Introduction

Bilateral facet dislocation (BFD) is a devastating consequence of cervical spine trauma [31], occurring most often during motor vehicle collisions, diving accidents, and falls [2, 5, 20]. The spinal cord injury rate is between 55 and 89%, with greater than 90% of patients presenting neurological symptoms [5, 12, 17, 20, 31]. Controversy exists regarding the specific ligaments injured [29]. Carrino et al. [8] performed a retrospective MRI study of 30 individuals who had sustained BFD, and reported ligament injury rates of 97% for the interspinous and supraspinous ligaments, 90% for the ligamentum flavum and disc, and 40% for the posterior and 26.7% for the anterior longitudinal ligaments. Despite the high injury severity, no clear treatment guidelines exist and the timing of closed reduction remains debatable. Some favor rapid reduction in an attempt to minimize cord injury [11, 31], while others believe the risk of disc herniation causing further cord compression upon reduction mandates pre-reduction imaging using MRI [6, 10]. Standard guidelines for cervical stabilization following reduction do not exist. The use of numerous treatment modalities such as halo vest immobilization, anterior

---

M. M. Panjabi · A. K. Simpson · P. C. Ivancic (✉) ·  
J. J. Yue  
Department of Orthopaedics and Rehabilitation,  
Yale University School of Medicine,  
333 Cedar Street, New Haven, CT 06520-8071, USA  
e-mail: paul.ivancic@yale.edu

A. M. Pearson  
Department of Orthopaedic Surgery,  
Dartmouth-Hitchcock Medical Center, Lebanon, NH, USA

Y. Tominaga  
Department of Orthopaedic Surgery,  
St. Marianna University School of Medicine,  
Kanagawa, Japan

plating, posterior fusion with plates or wires, or a combination of anterior and posterior fusion, indicates that the optimal treatment regimen has yet to be established [5, 12, 20, 25, 31]. These controversies may be due to poor understanding of the high-speed facet motions during dislocation that cause the wide range of ligamentous injury severity observed clinically.

Various motion patterns have been hypothesized to cause BFD, including hyperflexion [7], axial rotation [24], and hyperextension [28]. In a classic radiographic study, Allen et al. [2] suggested BFD as a flexion–distraction injury, and that the posterior ligaments may fail due to excessive strain, while compression injuries may occur to the anterior vertebral bodies and disc. This injury mechanism description is widely accepted [30], however no experimental evidence exists to support it.

Previous *in vitro* biomechanical models of BFD are limited to quasi-static loading or manual ligament transection. Roaf [24] applied compressive forces and axial torque to functional spinal units to produce dislocation, however, neither the loading rate nor the dislocation type were specified. Beatson [4] created dislocations using whole cervical spine specimens, and reported ruptures of the interspinous, capsular, and posterior longitudinal ligaments and annular fibers, though neither the high speed loading nor motion patterns were reported. Bauze and Ardran [3] applied flexion and compression loading to whole cervical spine specimens that were immobilized inferior to C5/6 to cause BFD at this spinal level. Interspinous, capsular, and anterior longitudinal ligament injuries were observed. These researchers hypothesized that combined anterior shear, flexion, and compression loading were necessary for dislocation. Others have transected cervical ligaments to manually create facet dislocation in order to study vertebral artery occlusion [26] or stabilization techniques [9, 16, 27].

In summary, no previous biomechanical study has investigated the kinematics of BFD by applying realistic high-speed loading to a human cervical spine model. Such data is necessary to better understand the injury mechanism and to identify the injured ligaments. The purpose of this study was to determine the kinematics of BFD using a biofidelic model consisting of a functional spinal unit with muscle force simulation.

## Materials and methods

### Anatomic coordinate systems

Two coordinate systems were used to express spinal motions during BFD:  $XYZ$ , the endplate coordinate system (Fig. 1a) and  $xyz$ , the facet coordinate system (Fig. 1b). A

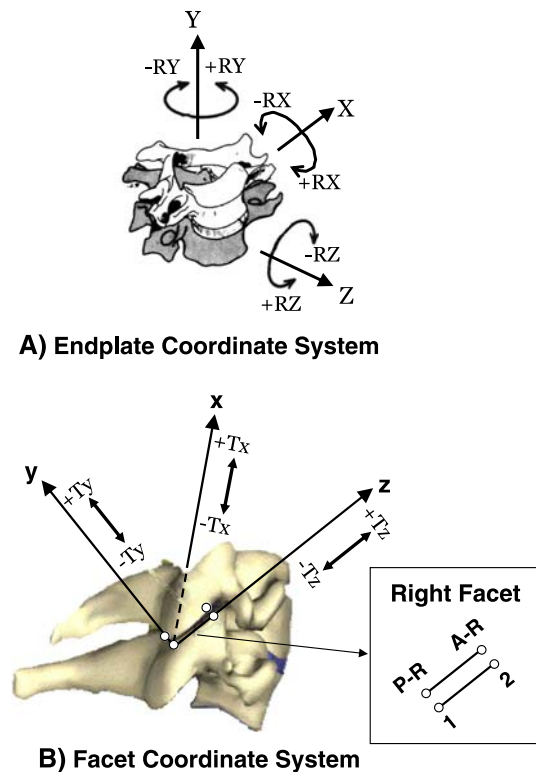


**Fig. 1** The coordinate systems and nomenclature for motions. **a** The endplate coordinate system was used to express the intervertebral rotations of flexion (+ $RX$ ), extension ( $-RX$ ), left (+ $RY$ ) and right ( $-RY$ ) axial rotation, and left ( $-RZ$ ) and right (+ $RZ$ ) lateral bending. **b** The facet coordinate system was used to express the facet translations of left (+ $Tx$ ) and right ( $-Tx$ ) lateral shear, axial separation (+ $Ty$ ) and compression ( $-Ty$ ), and anterior (+ $Tz$ ) and posterior ( $-Tz$ ) sliding. Shown for the right facet joint, the anterior and posterior aspects of the upper facet were defined by points A-R and P-R, respectively, while the anterior and posterior aspects of the lower facet were defined by points 2 and 1, respectively. Similar four points were also selected on the left facet joint

lateral radiograph of each specimen in the neutral posture (Fig. 2), together with radio-opaque scale markers positioned in the mid-sagittal plane and vertebral motion tracking flags was used to define the coordinate systems. The endplate coordinate system had its origin fixed at the posteroinferior corner of the lower vertebral body. The positive  $Z$ -axis for the endplate coordinate system was oriented anteriorly through the anteroinferior corner of the lower vertebral body, while the  $z$ -axis for the facet coordinate system was parallel to the facet surface of the superior facet of the lower vertebra. The positive  $Y$ - and  $y$ -axes were oriented superiorly and the positive  $X$ - and  $x$ -axes to the left.

### Specimen preparation

Four fresh-frozen human osteoligamentous cervical spine specimens (C3 to T1) were carefully dissected of all non-osteoligamentous soft tissues. The average age of the

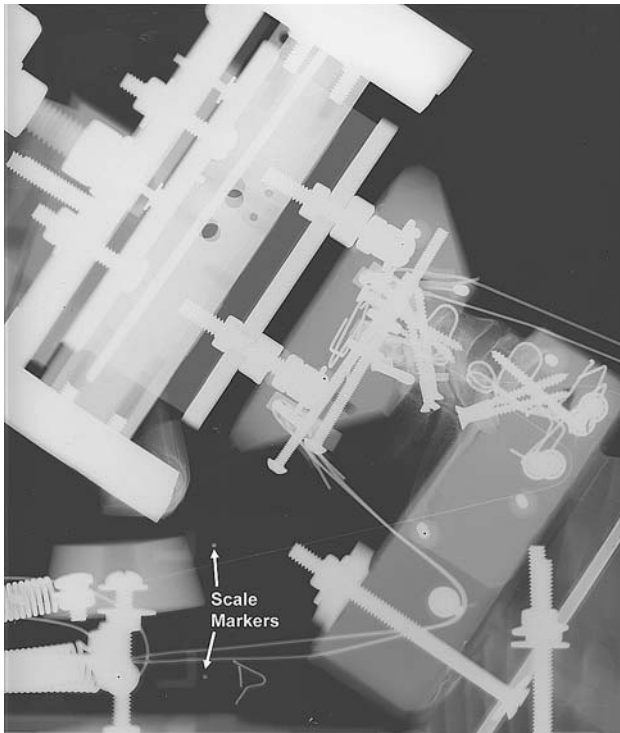


**Fig. 2** Lateral radiograph of the functional spinal unit (specimen #8; C5/6) mounted atop an extension wedge on the sled, with radio-opaque scale markers

specimens was 62 years (range 57–79 years) and there were two male and two female donors (Table 1). Other than normal age-related degenerative changes, the specimens had no history of cervical spine injury or disease that could have affected the osteoligamentous structures. The specimens were dissected into C3/4, C5/6, and C7/T1 functional spinal units (FSUs) resulting in four FSUs at each spinal level. Each FSU was mounted in resin at the upper and lower vertebrae such that the superior endplate of the lower vertebra was tilted anteriorly by  $12.5^\circ$  (SD  $6.2^\circ$ ). The vertebrae were rigidly secured within the mounts using screws and wiring [19], as shown in the lateral radiograph (Fig. 2). Motion tracking flags, each with three non-collinear markers, were rigidly fixed to both mounts. The lower mount was rigidly fixed to a  $55^\circ$  extension wedge on a custom built sled apparatus (Fig. 3). A mass of 3.3 kg with sagittal, horizontal, and frontal plane moments of inertia of 0.019, 0.014, 0.015  $\text{kg m}^2$ , respectively, was rigidly attached to the upper mount. The average (SD) coordinates of its center of mass in the neutral posture, expressed in the endplate coordinate system of the lower vertebra, were  $-12.4$  (19.7) mm for Z, 153.9 (7.1) mm for Y, and 0.0 (0.0) for X. The FSU and mass were stabilized using simulated compressive muscle forces, applied via bilateral cables originating from the upper mount at the four locations indicated in Fig. 3. Each cable was anchored

to a separate preloaded spring, with a stiffness of 4.0 N/mm. Cables 1 and 3 were connected directly to the springs, while cables 2 and 4 ran through pulleys within the lower mount. The preloads were 15 N in cables 1 and 4 and 30 N in cables 2 and 3, resulting in an intervertebral compressive preload of 180 N. This preload is in good agreement with the estimated in vivo C4/5 compression of 122 N in the relaxed posture [18]. This constituted the BFD model. It was developed through extensive preliminary trials and was found to consistently produce BFD.

#### Facet dislocation and monitoring

Horizontal acceleration of increasing severity was applied to the lower mount with frontal impact (Fig. 3) using a previously developed bench-top sled apparatus [22] until BFD was achieved. An accelerometer (part no. ADXL250JQC, Analog Devices, Norwood, MA, USA), oriented along the direction of impact, was fixed to the sled and measured its acceleration. The measured peak impact accelerations for each specimen are listed in Table 1. The three-dimensional coordinates of the flag markers were calculated in the ground coordinate system using digital stereophotography with two high-speed digital cameras recording at 500 frames/s (MotionPRO, Redlake MSAD, San Diego, CA, USA), and the Direct Linear Transformation technique [1, 23]. To calibrate the cameras, a custom calibration cage was photographed. Following each impact, the specimen was visually inspected to identify macroscopic ligamentous injury, if any. BFD was confirmed using fluoroscopy.

#### Facet geometry and kinematics

The distances from the mid-sagittal plane to the left and right facets were measured following BFD using a precision caliper (resolution 0.01 mm, Mitutoyo American Corp., Aurora, IL, USA). These data were used together with the coordinates of the vertebral flag marker centers and the lateral radiograph to develop three-dimensional geometric rigid body relationships between the flag markers and points on the facets. These relationships were superimposed onto the neutral posture frame of the high-speed movie. For each subsequent frame, custom Matlab software (The Mathworks Inc., Natick, MA, USA) automatically calculated the three-dimensional flag marker coordinates and translations, and intervertebral Euler angles in the sequence *RX*, followed by *RY* and *RZ*. The intervertebral rotations of flexion (*+RX*), extension (*-RX*), left (*+RY*) and right (*-RY*) axial rotation, and left (*-RZ*) and right (*+RZ*) lateral bending were expressed in the endplate coordinate system (Fig. 1a). For facet translations, two points were defined on each inferior facet of the upper

**Table 1** Macroscopic injuries and specimen demographics

| Cervical specimen | Age/gender | ID # | FSU                             | Measured peak impact acceleration (g) | Injuries following each impact                 |      |  |
|-------------------|------------|------|---------------------------------|---------------------------------------|--|------|--|
| A                 | 79/M       | 1    | C3/4                            | 7.2                                   | SSL, ISL, and LF ruptures                      |      |  |
|                   |            |      |                                 | 8.4                                   | Bilateral posterior CL rupture                 |      |  |
|                   |            |      |                                 | 9.9                                   | Annulus rupture and BFD                        |      |  |
|                   |            | 2    | C5/6                            | n/a                                   | Failed: complete ligament ruptures without BFD |      |  |
|                   |            |      |                                 | 3                                     | C7/T1  | 9.2  | ISL, LF, bilateral posterior CLs, and posterior annulus ruptures |
|                   |            |      |                                 |                                       |  | 9.9  | ALL and complete bilateral CL ruptures                           |
|                   |            |      |                                 |                                       |  | 10.2 | Complete annulus rupture   |
| 11.1              | BFD        |      |                                 |                                       |  |      |  |
| B                 | 57/F       | 4    | C3/4                            | 5.3                                   | ISL and LF ruptures                            |      |  |
|                   |            |      |                                 | 7.8                                   | Right posterior CL rupture                     |      |  |
|                   |            |      |                                 | 9.2                                   | Left posterior CL rupture                      |      |  |
|                   |            |      |                                 | 9.9                                   | Bilateral complete CL ruptures                 |      |  |
|                   |            |      |                                 | 11.6                                  | BFD  |      |  |
|                   |            | 5    | C5/6                            | 8.6                                   | ISL and LF ruptures                            |      |  |
|                   |            |      |                                 | 9.1                                   | Right posterior CL rupture                     |      |  |
|                   |            |      |                                 | 9.5                                   | Left posterior CL rupture                      |      |  |
|                   |            | 6    | C7/T1                           | n/a                                   | Failed: complete ligament ruptures without BFD |      |  |
|                   |            |      |                                 | 7                                     | C3/4   | 5.4  | ISL, LF, and bilateral posterior CL ruptures                     |
|                   |            |      |                                 |                                       |  | 7.7  | BFD  |
| 8                 | C5/6       | 9.3  | ISL and LF ruptures             |                                       |  |      |  |
|                   |            | 9.6  | Bilateral posterior CL ruptures |                                       |  |      |  |
|                   |            | 10.1 | No further injury               |                                       |  |      |  |
|                   |            | 10.6 | BFD                             |                                       |  |      |  |
|                   |            | 10.7 | BFD                             |                                       |  |      |  |
| C                 | 73/M       | 9    | C7/T1                           | 5.4,8.9,10.1,10.3                     | Information not available                      |      |  |
|                   |            |      |                                 | 10.7                                  | BFD  |      |  |
|                   |            |      |                                 | 10.7                                  | BFD  |      |  |
| D                 | 39/F       | 10   | C3/4                            | 5.5                                   | ISL, LF, and left posterior CL ruptures        |      |  |
|                   |            |      |                                 | 7.6                                   | Complete bilateral CL ruptures                 |      |  |
|                   |            |      |                                 | 8.3                                   | BFD  |      |  |
|                   |            | 11   | C5/6                            | 5.6                                   | ISL, LF, and bilateral posterior CL ruptures   |      |  |
|                   |            |      |                                 | 7.6                                   | BFD  |      |  |
|                   |            | 12   | C7/T1                           | 7.6                                   | ISL, LF, and bilateral posterior CL ruptures   |      |  |
| 9.3               | BFD        |      |                                 |                                       |  |      |  |

A total of 12 functional spinal units (FSUs) were prepared from four cervical spine specimens. Ten FSUs achieved bilateral facet dislocation (BFD), while two failed to do so. Macroscopic injuries were documented in the ligamentum flavum (LF) and anterior longitudinal (ALL), capsular (CL), interspinous (ISL) and supraspinous (SSL) ligaments

vertebra: A-R and P-R were the anterior and posterior corners of the right facet, respectively (Fig. 1b insert), and, similarly, there were points A-L and P-L for the left facet. The translations of these points were calculated relative to respective points on the superior facets of the lower vertebra using the rotation data, vertebral flag marker translations, and the geometrical rigid body relationships [14]. The facet translations were left (+Tx) and right (-Tx) lateral shear, axial separation (+Ty) and compression (-Ty), and anterior (+Tz) and posterior (-Tz) sliding, expressed in the facet coordinate system. The intervertebral rotations and

facet translations during BFD were zeroed relative to the neutral posture. The average (SD) errors were 0.28 mm (0.18 mm) for facet translation and  $-0.06^\circ$  (0.17°),  $0.06^\circ$  (0.18°), and  $0.07^\circ$  (0.12°) for the rotations RX, RY, and RZ, respectively [14].

#### Data analyses

The kinematic data were low pass digitally filtered at a cut-off frequency of 30 Hz. Residual and Fourier analyses demonstrated that most of the signal power was contained

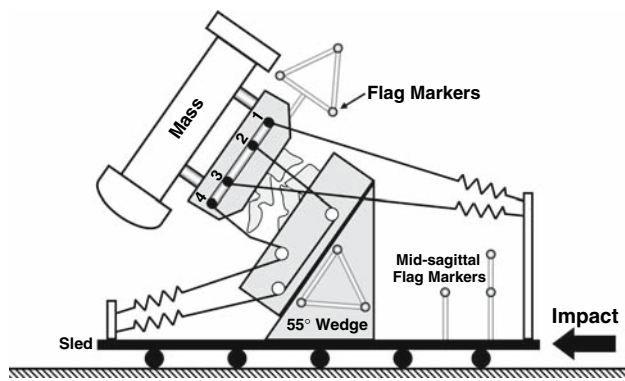


**Fig. 3** Schematic of the functional spinal unit model with mass, stabilized with muscle force replication, ready for simulated bilateral facet dislocation. Bilateral muscle force cables originated from the upper mount at the four indicated locations. The flag markers are also shown

under 20 Hz. The motion peaks were determined during the impact that caused BFD (Table 1) during the flexion period (from the onset of the sled acceleration to the return of the upper vertebra to neutral posture). The occurrence times of all motion peaks, relative to the onset of the horizontal acceleration of the lower vertebra, were also determined.

#### Statistics

Since no significant differences were observed in the average motion peaks among the three spinal levels, data

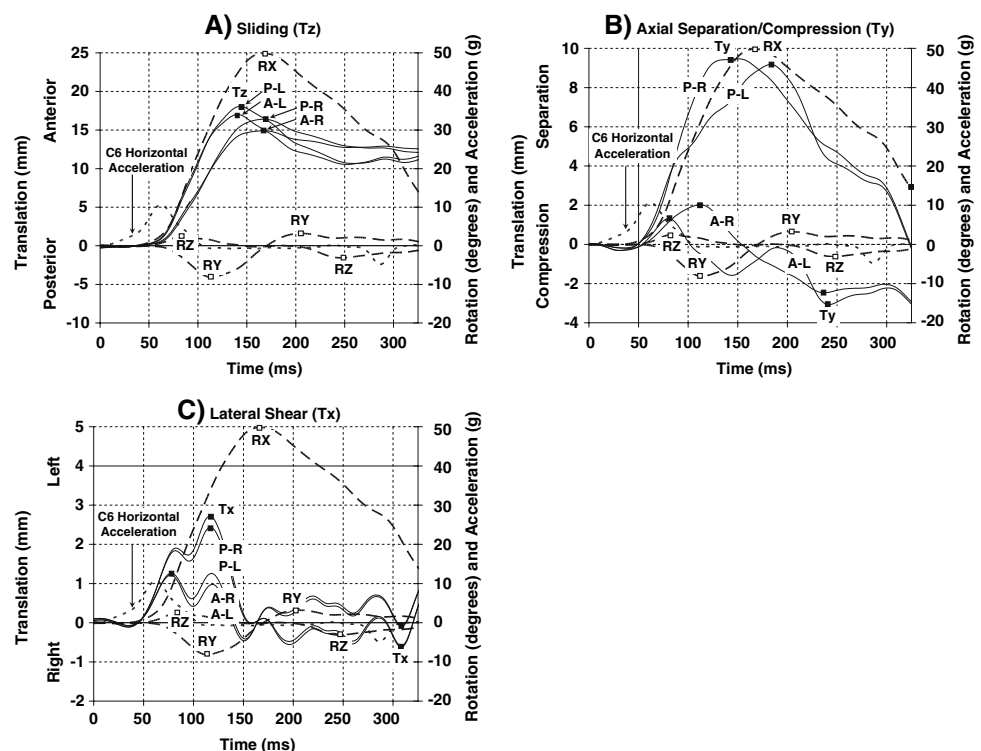
from all spinal levels were combined for subsequent analyses. Single factor, non-repeated measures ANOVA ( $P < 0.05$ ) and Bonferonni pair-wise post-hoc tests (Minitab Rel. 13, Minitab, State College, PA, USA) were used to determine differences in the average peak facet translations (anterior and posterior, left and right facet corners) and rotations ( $RX$ ,  $RY$ , and  $RZ$ ). Adjusted  $P$ -values were computed based upon the 40 post hoc tests performed.

#### Results

##### A representative example

In this example of BFD (Fig. 4), the measured peak horizontal acceleration causing the BFD was 10.6 g and the acceleration pulse duration was 104 ms. Following impact, coupled intervertebral rotations were observed, consisting of  $+RX$ ,  $-RY$ , and  $+RZ$  followed by  $+RX$ ,  $+RY$ , and  $-RZ$ . The  $+Tz$  peaks occurred first in the left facet, reaching 17.0 and 18.1 mm at A-L and P-L, respectively (Fig. 4a). The  $+Ty$  peaks (Fig. 4b) were highest in the posterior facet edges, P-L and P-R. Subsequently, lower  $-Ty$  peaks were observed for A-L and A-R. The  $+Tx$  peaks were higher for facet edges, P-L and P-R, as compared to the anterior (Fig. 4c). Notice that the initial non-sagittal rotations of  $-RY$  and  $+RZ$  caused greater  $+Tz$  in the left facet (A-L and P-L, Fig. 4a), as compared to the right facet, and greater

**Fig. 4** A representative example of simulated bilateral facet dislocation (specimen #8; C5/6; 10.6 g) showing the facet translations and intervertebral rotations versus time: **a** sliding ( $Tz$ ), **b** axial separation/compression ( $Ty$ ), and **c** lateral shear ( $Tx$ ) at the anterior-left (A-L), anterior-right (A-R), posterior-left (P-L), and posterior-right (P-R) facet edges. Note that the scales are  $-10$  to  $25$  mm for  $Tz$ ,  $-4$  to  $10$  mm for  $Ty$ , and  $-2$  to  $5$  mm for  $Tx$ . The peaks are indicated with closed squares for the facet translations and open squares for the rotations of flexion-extension ( $RX$ ), axial rotation ( $RY$ ), and lateral bending ( $RZ$ ). The C6 posterior horizontal acceleration is also shown. For the nomenclature, please see Fig. 1



+ $T_x$  in the posterior facet edge (P-L and P-R, Fig. 4c), as compared to the anterior.

### The ten specimens

BFD was achieved in 10 of the 12 FSUs, as documented by fluoroscopy (Table 1). The measured peak frontal impact acceleration required to produce BFD varied among specimens, and ranged between 7.7 and 11.1 g. The average acceleration pulse duration was 97 ms. The visual inspections following each impact demonstrated macroscopic ligament injuries specific to each specimen consisting of ruptures of the supraspinous, interspinous, capsular, or anterior longitudinal ligaments, ligamentum flavum or annular fibers.

The average peak motions are presented in graphical form, together with significant differences between anatomical location for facet translations (anterior and posterior, left and right facet corners) and between rotation directions ( $RX$ ,  $RY$ , and  $RZ$ ). Peak + $RX$  of  $63.1^\circ$  significantly exceeded ( $P < 0.05$ ) all other rotation peaks (Fig. 5a). The highest peak + $T_z$  of 22.0 mm occurred in the posterior edge of the left facet and could not be statistically differentiated from the other + $T_z$  peaks (Fig. 5b). The + $T_y$  peak, reaching 7.9 mm at the posterior edge of the left facet, was significantly greater than the + $T_y$  peaks at the anterior facet edges (Fig. 5c). The - $T_y$  peaks reached 9.9 and 7.4 mm at the anterior and posterior edges of the left facet, respectively (Fig. 5d). The greatest + $T_x$  and - $T_x$  peaks were 2.0 and 3.6 mm, respectively (Fig. 5e, f).

The average times at which the sagittal motion peaks were attained are presented in tabular form, ordered chronologically for the left and right facets (Table 2a, b). The + $T_y$  peaks at the anterior followed by the posterior facet edge occurred first, and then the + $RX$  and + $T_z$  peaks. Lastly, the - $T_y$  peaks occurred, first at the anterior followed by the posterior facet edges. All peaks occurred prior to the average onset of sled deceleration (280 ms) with the exception of the - $T_y$  peaks at the posterior facet edges.

### Discussion

Bilateral facet dislocation in the cervical spine causes neurological symptoms in greater than 90% of patients [5, 12, 17, 20, 31]. Ours is the first study to provide comprehensive three-dimensional facet translations and intervertebral rotations during high-speed BFD of a human functional spinal unit model with muscle force simulation. Frontal impact of increasing severity was applied to the lower vertebra until BFD was achieved. The present macroscopic ligament injuries documented after each impact (Table 1) are consistent with those sustained in real-life BFD [8, 29], with the

most injuries occurring to the ligamentum flavum and interspinous and supraspinous ligaments. The sagittal motion peaks were consistent chronologically among specimens, however the chronology of the non-sagittal motion peaks was specimen-specific.

The temporal analysis of the sagittal motions at the right facet joint during BFD was presented in Table 2b, and is illustrated in Fig. 6. Peak axial separation occurred first, greater at the posterior facet corner, as compared to anterior, as the upper facet slid anteriorly relative to the lower facet and flexed (Fig. 6b). Peak flexion rotation occurred next, as the upper facet continued to slide anteriorly, axial separation at the posterior facet corner decreased, and compression occurred at the anterior facet corner (Fig. 6c). Peak anterior sliding was then observed as axial separation at the posterior facet corner continued to decrease (Fig. 6d). Lastly, peak axial compression occurred, greatest at the anterior corner (Fig. 6e), as the upper facet had jumped over the lower facet and was locked in the intervertebral foramina, resulting in the BFD status observed clinically.

There are some limitations of the present model. Being an in vitro study, the effects of the neuromuscular control system were not included. The muscle force simulation, adopted from a previous study [13], provided biofidelic compressive loads (Fig. 3). While direct head loads can cause real-life BFD during diving accidents or falls, these loads were not simulated in the present model. Production of BFD in a whole cervical spine model using direct or inertial head loads was beyond the scope of the present study. The horizontal acceleration applied to the lower vertebra of the present model mounted atop an extension wedge produced inertial loading necessary to consistently produce BFD (Table 1). The incremental trauma approach was used and facet joint kinematics were reported for the minimum impact acceleration required to cause BFD. In real-life BFD, greater energy may be transferred to the cervical spine, resulting in higher peak motions. To compute the facet kinematics, it was assumed that the motion tracking flag and vertebra constitute a rigid body. Rigid fixation of the vertebrae within the mounts using screws and wiring [19] (Fig. 2) ensured no loosening at the vertebrae-mount interfaces.

There exist few biomechanical studies of BFD with which our results may be compared, with most being limited by unrealistic quasi-static loading or manual ligament transection [3, 4, 24]. These previous models have been used to determine ligament injuries, investigate loading directions responsible for BFD, and to study vertebral artery occlusion [26] and stabilization techniques [9, 16, 27]. We have recently reported spinal canal narrowing during simulated high-speed BFD of the functional spinal unit model with muscle force replication

**Fig. 5** Average peak (a) intervertebral rotations and facet translations of (b) anterior sliding (+ $T_z$ ), (c) axial separation (+ $T_y$ ), (d) axial compression (- $T_y$ ), (e) left lateral shear (+ $T_x$ ), and (f) right lateral shear (- $T_x$ ). Significant differences ( $P < 0.05$ ) resulting from the pair-wise comparisons are indicated with brackets

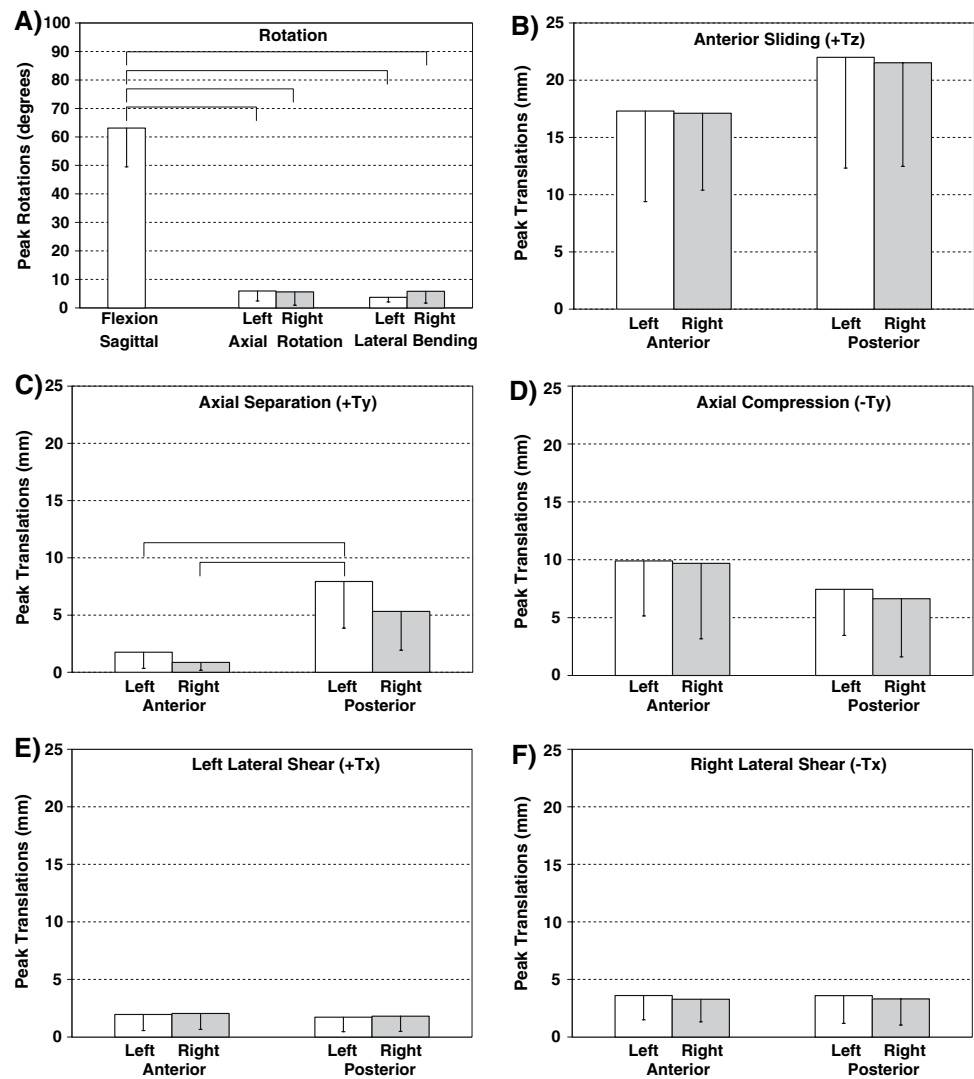


**Table 2** Event times

| (a) Left facet joint |              |           | (b) Right facet joint |              |           |
|----------------------|--------------|-----------|-----------------------|--------------|-----------|
| Time                 | Event        | Magnitude | Time                  | Event        | Magnitude |
| 88 (30)              | + $T_y$ Ant  | 1.8       | 81 (27)               | + $T_y$ Ant  | 0.9       |
| 134 (44)             | + $T_y$ Post | 7.9       | 122 (57)              | + $T_y$ Post | 5.3       |
| 157 (27)             | + $T_z$ Post | 22.0      | 158 (19)              | + $RX$       | 63.1      |
| 158 (19)             | + $RX$       | 63.1      | 173 (76)              | + $T_z$ Ant  | 17.1      |
| 168 (78)             | + $T_z$ Ant  | 17.3      | 175 (75)              | + $T_z$ Post | 21.5      |
| 256 (82)             | - $T_y$ Ant  | 9.9       | 231 (77)              | - $T_y$ Ant  | 9.7       |
| 295 (67)             | - $T_y$ Post | 7.4       | 294 (48)              | - $T_y$ Post | 6.6       |

Average (SD) times in milliseconds, in chronological order, at which the sagittal motion peaks were attained relative to the onset of the horizontal acceleration of the lower vertebra during BFD for (a) the left facet joint and (b) the right facet joint. The average magnitudes of the motion peaks (degrees or mm) are also provided. Translations are given at the anterior (ant) and posterior (post) facet edges

[15]. Peak spinal canal narrowing, and hence the greatest potential for cord compression injury, occurred between 71 and 97 ms following impact, on average. The present

temporal analyses of facet joint kinematics indicates that anterior sliding of the upper facet relative to the lower, together with flexion rotation and axial facet separation,

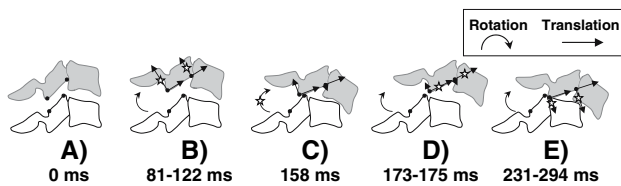


**Fig. 6** Schematic indicating key events during bilateral facet dislocation, based upon the temporal analysis of sagittal motion peaks at the right facet joint (Table 2b). **a** The neutral position. **b** Peak axial separation was observed, greatest at the posterior edge, while the upper facet slid anteriorly relative to the lower facet. **c** Peak flexion rotation occurred as the upper facet continued to slide anteriorly. **d** Peak anterior sliding was observed as the posterior axial separation continued to decrease and anterior axial compression was observed. **e** Peak axial compression was observed, greatest at the anterior edge. Note that the translation and rotation magnitudes are not drawn to scale

may be the primary motions that cause cord compression injury during BFD.

The present data, in addition to providing insight into facet kinematics during BFD, may be used to discuss potential neck loads necessary to cause BFD. White and Panjabi [30] hypothesized that loading consisting of a large flexion moment combined with a small axial compression force may cause the facet translations of anterior sliding and axial separation necessary to cause BFD. Panjabi et al. [21] reported the intervertebral motions of C2/3 to C7/T1 spinal levels in response to quasi-static forces, and these data may be used to further understand mechanisms of BFD. They found that axial tension and anterior shear forces, each independently applied, caused flexion rotation, axial separation, and anterior sliding, while an axial compression force caused motions in the opposite directions. Applying these load-motion results to the present data indicates that initial facet loading may consist of a combined flexion moment and anterior shear force causing the observed motions of flexion rotation, anterior sliding, and axial separation. Subsequently, these loads, in addition to a compressive force, may cause the observed motions of flexion rotation, anterior sliding, and axial compression.

The non-sagittal motions observed in the present study imply that either the left or right facet capsule is stretched more than the other during BFD, initiating a unilateral injury. The average non-sagittal motion peaks reached nearly  $6.0^\circ$  for both axial rotation and lateral bending and 3.6 mm for lateral shear (Fig. 5). These non-sagittal motions may be due to non-symmetrical spinal anatomy and ligament mechanical properties or slight lateral offset of the upper mass prior to impact. We believe that these factors improved the clinically relevant biofidelity of our model. Cervical spine motions during real-life BFD are most likely not limited to the sagittal plane, but consists of complex three-dimensional motions during unanticipated

motor vehicle collisions, diving accidents, and falls [2, 5, 20]. As such, the motions of the left and right facet joints may differ, causing unilateral dislocation either solely or prior to BFD. The present three-dimensional motion data provide insight into the complex mechanism of BFD.

## Conclusions

The present study documented the three-dimensional facet translations and intervertebral rotations during simulated high-speed BFD of the functional spinal unit model with muscle force simulation. We observed that peak facet separation occurred first, and was significantly greater at the left posterior facet edge, as compared to the anterior edges. Subsequently, peak flexion rotation and anterior facet sliding occurred, followed by peak facet compression. These data help improve our understanding of the three-dimensional motions during BFD. Our model, which includes realistic high-speed loading, consistently produced BFD and may be used to investigate spinal cord [15], nerve root, ganglion, and vertebral artery occlusion, and ligament strains during BFD. The present specimens, having sustained realistic ligamentous injuries due to simulated BFD, may be used to evaluate, *in vitro*, the effectiveness of clinically relevant stabilization techniques such as anterior cervical discectomy and fusion, posterior fusion, or both.

**Acknowledgment** This research was supported by a grant from the Cervical Spine Research Society.

## References

1. Abdel-Aziz YI, Karara HM (1971) Direct linear transformation from comparator coordinates into object space coordinates in close-range photogrammetry. Symposium on close-range photogrammetry. University of Illinois
2. Allen BL Jr, Ferguson RL, Lehmann TR, O'Brien RP (1982) A mechanistic classification of closed, indirect fractures and dislocations of the lower cervical spine. *Spine* 7:1–27
3. Bauze RJ, Ardran GM (1978) Experimental production of forward dislocation in the human cervical spine. *J Bone Joint Surg Br* 60-B:239–245
4. Beatson T (1963) Fractures and dislocations of the cervical spine. *J Bone Joint Surg (Br)* 45-B:21–35
5. Bedbrook GM, Sakae T (1982) A review of cervical spine injuries with neurological dysfunction. *Paraplegia* 20:321–333
6. Berrington NR, van Staden JF, Willers JG, van der Westhuizen J (1993) Cervical intervertebral disc prolapse associated with traumatic facet dislocations. *Surg Neurol* 40:395–359
7. Braakman R, Vinken PJ (1967) Unilateral facet interlocking in the lower cervical spine. *J Bone Joint Surg Br* 49:249–257
8. Carrino JA, Manton GL, Morrison WB et al (2006) Posterior longitudinal ligament status in cervical spine bilateral facet dislocations. *Skeletal Radiol* 35:510–514



9. Coe JD, Warden KE, Sutterlin CE 3rd, McAfee PC (1989) Biomechanical evaluation of cervical spinal stabilization methods in a human cadaveric model. *Spine* 14:1122–1131
10. Doran SE, Papadopoulos SM, Ducker TB, Lillehei KO (1993) Magnetic resonance imaging documentation of coexistent traumatic locked facets of the cervical spine and disc herniation. *J Neurosurg* 79:341–345
11. Grant GA, Mirza SK, Chapman JR et al (1999) Risk of early closed reduction in cervical spine subluxation injuries. *J Neurosurg* 90:13–18
12. Hadley MN, Fitzpatrick BC, Sonntag VK, Browner CM (1992) Facet fracture-dislocation injuries of the cervical spine. *Neurosurgery* 30:661–666
13. Ivancic PC, Panjabi MM, Ito S, Cripton PA, Wang JL (2005) Biofidelic whole cervical spine model with muscle force replication for whiplash simulation. *Eur Spine J* 14:346–355
14. Ivancic PC, Wang JL, Panjabi MM (2006) Calculation of dynamic spinal ligament deformation. *Traffic Inj Prev* 7:81–87
15. Ivancic PC, Pearson AM, Tominaga Y et al (2007) Mechanism of cervical spinal cord injury during bilateral facet dislocation. *Spine* (in press)
16. Kim SM, Lim TJ, Paterno J, Park J, Kim DH (2004) A biomechanical comparison of three surgical approaches in bilateral subaxial cervical facet dislocation. *J Neurosurg Spine* 1:108–115
17. Lintner DM, Knight RQ, Cullen JP (1993) The neurologic sequelae of cervical spine facet injuries. The role of canal diameter. *Spine* 18:725–729
18. Moroney SP, Schultz AB, Miller JA (1988) Analysis and measurement of neck loads. *J Orthop Res* 6:713–720
19. Nuckley DJ, Hertsted SM, Eck MP, Ching RP (2005) Effect of displacement rate on the tensile mechanics of pediatric cervical functional spinal units. *J Biomech* 38:2266–2275
20. O'Brien PJ, Schweigel JF, Thompson WJ (1982) Dislocations of the lower cervical spine. *J Trauma* 22:710–4
21. Panjabi MM, Summers DJ, Pelker RR et al (1986) Three-dimensional load-displacement curves due to forces on the cervical spine. *J Orthop Res* 4:152–161
22. Panjabi MM, Cholewicki J, Nibu K, Babat LB, Dvorak J (1998) Simulation of whiplash trauma using whole cervical spine specimens. *Spine* 23:17–24
23. Reinschmidt C, Bogert TVD (1997) KineMat: custom Matlab software. Human Performance Laboratory, The University of Calgary <http://www.isbweb.org/software/>
24. Roaf R (1960) A study of the mechanics of spinal injuries. *J Bone Joint Surg (Br)* 42-B:810–823
25. Sears W, Fazl M (1990) Prediction of stability of cervical spine fracture managed in the halo vest and indications for surgical intervention. *J Neurosurg* 72:426–432
26. Sim E, Vaccaro AR, Berzlanovich A, Pienaar S (2000) The effects of staged static cervical flexion–distraction deformities on the patency of the vertebral arterial vasculature. *Spine* 25:2180–6
27. Sutterlin CE 3rd, McAfee PC, Warden KE, Rey RM Jr, Farey ID (1988) A biomechanical evaluation of cervical spinal stabilization methods in a bovine model. Static and cyclical loading. *Spine* 13:795–802
28. Taylor A, Blackwood W (1948) Paraplegia in hyperextension cervical injuries with normal radiographic appearances. *J Bone Joint Surg (Br)* 30-B:245–248
29. Vaccaro AR, Madigan L, Schweitzer ME et al (2001) Magnetic resonance imaging analysis of soft tissue disruption after flexion–distraction injuries of the subaxial cervical spine. *Spine* 26:1866–1872
30. White AA 3rd, Panjabi MM (1990) Clinical biomechanics of the spine. J.B. Lippincott, Philadelphia
31. Wolf A, Levi L, Mirvis S et al (1991) Operative management of bilateral facet dislocation. *J Neurosurg* 75:883–890